Optical Materials 112 (2021) 110777

Contents lists available at ScienceDirect

Optical Materials

journal homepage: http://www.elsevier.com/locate/optmat

Research Article

Thermo-optic refraction in MoS_2 medium for "Normally on" all optical switch

Pritam P. Shetty [a], Mahalingam Babu [a], Dmitrii N. Maksimov [b,c], Jayachandra Bingi [a,*]

[a] Bio-inspired Research and Development (BiRD) Laboratory, Photonic Devices and Sensors (PDS) Laboratory, Indian Institute of Information Technology Design and Manufacturing (IIITDM), Kancheepuram, Chennai, 600127, India
[b] Kirensky Institute of Physics, Federal Research Center KSC SB RAS, 660036, Krasnoyarsk, Russia
[c] Siberian Federal University, Krasnoyarsk, 660041, Russia

ARTICLE INFO

Keywords:
Thermal lensing
Optical modulation
2D nanomaterials
Molybdenum disulfide
All optical switch
Thermal lens spectroscopy

ABSTRACT

Two dimensional (2D) nanomaterials like Molybdenum disulfide (MoS_2) have been drawing a lot of interest due to their excellent nonlinear optical response. In this research we study thermal lens formation in MoS_2 nanoflakes dispersion using mode mismatched pump probe configuration. Observation of the pump and probe beam intensity patterns gave visual insights on time evolution of photothermal lens formation. Effect of MoS_2 nanoflakes concentration on thermo-optic properties of dispersions were studied using thermal lens spectroscopy technique. Further, a thermo-optic refraction based technique to measure thermal lens size is proposed. Thermal lens region size increased with increase in pump power. The observed thermal lens modulation is applied to demonstrate 'normally on' all optical switch which showed excellent modulation of output beam signal by pump beam.

1. Introduction

Molybdenum disulfide (MoS_2) is a 2D nanomaterial and lately has been under lot of attention by research community. A monolayer MoS_2 has two planes of hexagonally arranged sulfur atoms and one plane of hexagonally arranged molybdenum atoms sandwiched between them [1]. MoS_2 is attractive due to its good thermodynamic [2], mechanical [3], optical properties [4,5], and semiconducting nature [6]. Owing to this, 2D MoS_2 finds its application in Biosensing [7], microelectronics [8], optoelectronics [9], catalysis [10], lubrication and non-linear optics [11,12]. Liquid phase exfoliation technique is widely used to produce high quality and quantity of MoS_2 nanoflakes solutions with each nanoflake comprising of one or few 2D layers of MoS_2 [13].

The optical Kerr effect is a phenomenon observed in some materials when an intense beam of light passes through them. This causes a change in the refractive index of material proportional to the local intensity of light. Further, this effect is also responsible of nonlinear optical effects like self-focusing/defocusing and spatial self-phase modulation (SSPM). SSPM causes the emerging beam from that material to self-interfere and have a concentric ring like intensity pattern (diffraction rings). The optical Kerr effect is also observed in MoS_2 dispersions [14,15]. Dynamics of SSPM has been studied theoretically by proposing different models or by observing changes in diffraction ring [15–17]. All optical switching using nanomaterial dispersions have been demonstrated, but output of these devices varies as a function of number of rings [18] or ring deformation [19]. This does not give a precise control over the output. We take the approach of thermo-optic refraction rather than diffraction for optical switch, this opens the possibility for scaling of the device to microlevel. Proposed device in micro-scale can have lower power consumption and higher response time. Srivastava et al. have demonstrated MoS_2 based micro optical device for ultra-fast optical switching in different pump probe configuration [20].

In this research we probe the region of interaction of pump laser beam with MoS_2 dispersions using a second diverging beam (probe beam). This gives us a visual insight into the dynamics of photothermal lens formation within MoS_2 dispersion and its effect on temporal diffraction ring evolution of the pump beam. The effect of pump beam power on the thermal lens region size is studied. Thermal lens spectroscopy (TLS) technique is used to calculate thermo-optic properties of the dispersions with varying concentration of MoS_2 nanoflakes. Further, a 'normally on' all-optical switch is demonstrated.

* Corresponding author.
E-mail addresses: bingi@iiitdm.ac.in, jayachandra@iiitk.ac.in (J. Bingi).

https://doi.org/10.1016/j.optmat.2020.110777
Received 15 September 2020; Received in revised form 26 November 2020; Accepted 21 December 2020
Available online 31 December 2020
0925-3467/

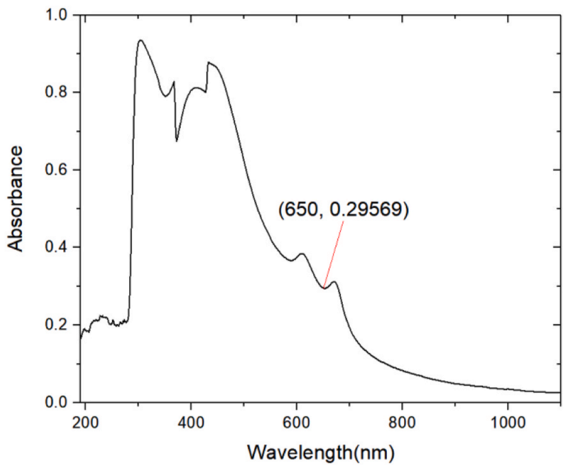

Fig. 1. Absorption spectrum of MoS_2 nanoflake dispersion.

2. Results and discussions

2.1. Material preparation and characterization

MoS_2 powder (98% pure) is grinded by Mortar and Pestel for 5 h using Methanol as solvent and dried for four days. 3%w/w Polyvinylpyrrolidone (PVP) polymer solution is prepared by mixing PVP with ethanol/acetonitrile blend as solvent. The solvent blend is prepared by mixing of ethanol and acetonitrile in ratio 1:1. MoS_2 dispersions were prepared by adding 2%w/w grinded MoS_2 to the PVP polymer solution. The PVP polymer acts as colloidal stabilizer. The dispersions are sonicated for 3 h. After sonication, dispersions were centrifuged for 2 h. Centrifugation allows bulk MoS_2 to settle at bottom and we can extract the colloidal solution with MoS_2 nanoflakes by pipetting. This freshly prepared MoS_2 dispersion is diluted by two-fold series dilution with addition of PVP solution thrice. These diluted samples are later used to study the changes in thermo-optic properties of dispersion as a function of the MoS_2 nanoflakes concentration.

The UV–Vis spectrum as shown in Fig. 1 indicates that the dispersions have broadband absorption in visible region (400–700 nm) and can be a prospective optical material in the visible region. In this research, light of 650 nm wavelength is used with the absorption coefficient of 0.681 cm^{-1}.

The dispersions were spin coated on glass slide for SEM analysis. As seen in Fig. 2 the nanoflakes had uniform size and average thickness of 153.5 nm ± 23 nm.

Evolution of thermal lens region and Quantifying its size.

The MoS_2 dispersion samples were poured into a glass cuvette of path length 1.5 mm. A collimated pump beam generated by a laser diode ($\lambda e = 650$ nm) is focused on the sample using lens L_1. The power of pump beam is controlled by a variable neutral density (ND) filter. A collimated beam from diode laser ($\lambda p = 650$ nm) is used for probe beam. Using lens L_2, probe beam of divergence 67 mrad is passed through focal point of the pump beam on the sample to study thermal lensing effect. The probe beam is passed through the sample at a small angle of $\sim 2^\circ$ with respect to the axis of the pump beam to separate the pump and probe intensity pattern on the screen.

When the pump beam is focused on MoS_2 dispersion, there is intense localized heat generation due to absorption by suspended nanoflakes. Three-dimensional thermal distribution at the focal point inside the sample can be approximated to have spherical gradient (assuming there is no convective heat flow in dispersion). This causes a corresponding spherical gradient refractive index change in the MoS_2 dispersion with a very low refractive index at the center. Due to intense radial refractive index change encountered by pump beam, it undergoes self-interference along the direction of propagation causing concentric diffraction rings on the screen as shown in Fig. 4. There are three stages found in time evolution of the thermal lens region when the pump beam and probe beam output from the sample is observed- *Symmetric diffraction rings*: The intensity distribution of probe beam forms a symmetric diffraction beam. This indicates there is no convective heat flow and a perfect spherical gradient refractive index distribution is formed at the pump beam waist. A tiny circular dark spot can be seen in the probe beam (Fig. 4). Strong localized heating by the pump beam causes a spherical gradient refractive index lens with low refractive index at the center and increasing along the radial distance. This thermal lens strongly diverges the part of probe beam encountered by it, causing a dark spot.

Asymmetric diffraction rings: As the pump beam waist radius (18.9 μm) is far smaller than the thermal lens region (~1 mm), the intensity distribution of the pump beam (diffraction rings) is very sensitive to any convective heat flow in dispersions. Hence when convective heat flow emerges, it is first indicated by collapsing of the diffraction ring in the pump beam but the dark spot in probe beam still appears circular.

Asymmetric dark spot: When equilibrium is reached between heat carried by convection and heat generation by the pump beam, a stable asymmetric dark spot can be seen in the probe beam. This dark spot in the probe beam along with the thermal plume due to convection can be clearly seen in Fig. 5. In Fig. 4 the intensity patterns of the asymmetric dark spot for all pump powers is taken at elapsed time of 3 s and does not represent the time of equilibrium. However, it is observed that the asymmetric dark spot formation is faster at higher pump powers.

By knowing the size of the dark spot, we can approximately calculate the diameter of the thermal lens region. It is assumed that there is no deflection of rays at the edge of the thermal lens region. Hence the probe rays emerging from the focal point of lens L_2 subtends an angle $\angle zxy$

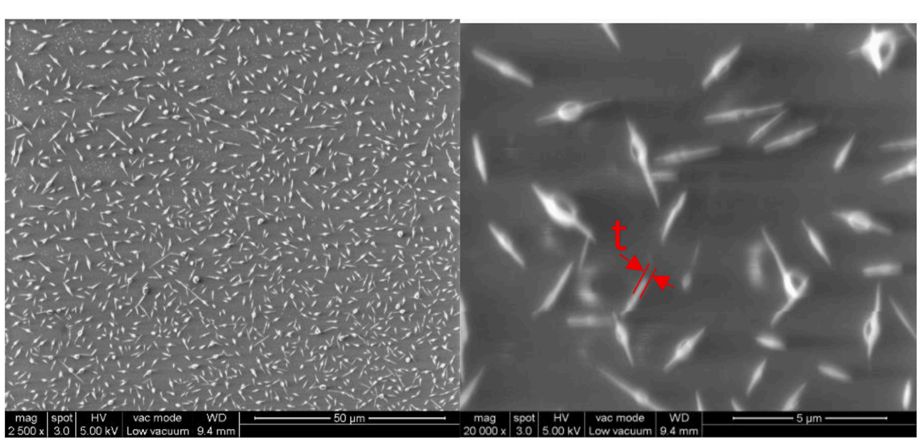

Fig. 2. SEM micrograph of thin films of MoS_2 nanoflakes dispersion on glass slide. (right)zoomed view.

Table 1
Variation of thermal lens size with pump power.

Pump power (mW)	r_{ds} (mm)	r_{TL} (mm)
35	10.145	0.96507
30	9.5	0.903712
25	9.3	0.884687
20	8.8	0.837123
15	8.3	0.789559
10	7.5	0.713457
5	6.25	0.594548

with distances r_{TL} and r_{DS} respectively (Fig. 5 inset). Here, r_{TL} and r_{DS} are the radius of the thermal lens region within the sample and the radius of the dark spot on the screen, respectively. Here r_{DS} is measured horizontally on the screen as dimensions in this direction is not affected by the convective flow in the dispersion. By using a simple relation, we can find the radius of the thermal lens region:

$$r_{TL} = \frac{a}{b} * r_{DS}$$

Time evolution of the thermal lens region and thermal lens size is recorded by varying the pump power from 5 to 35 mW as shown in Fig. 4 and Table 1.

It can be observed from Fig. 4 that as the pump power is increased the time taken to form the asymmetric diffraction ring reduces i.e. the convection flow is stronger. At pump power less than 10 mW, the diffraction rings as well as the dark spot remain symmetric signifying there is very low thermal convection. The number of diffraction rings in the pump beam reduces with reduction in the pump power showing that the radial thermal gradient is also reduced. This is confirmed in Table 1 where the thermal lens size is reduced by 38.4% as the pump power is reduced from 35 mW to 5 mW. Fig. 6 shows a linear dependence of the thermal lens size on the pump power. Hence, for micro-optical devices with few layers of MoS_2, the pump power requirement will be low. This will be ideal for low power device application.

Thermal lens spectroscopic (TLS) analysis of MoS_2 dispersion.

The MoS_2 dispersion were analyzed by TLS method in dual beam mode mismatched configuration as shown in the experimental setup in Fig. 3. To record the thermal lens (TL) signal I(t), a photodiode connected to an oscilloscope is placed at the center of the dark spot in the probe beam transmitted through sample. By fitting an analytical expression based on the theoretical model by J Shen et al. [21] to experimental TL signal data, various thermal and optical parameters of the MoS_2 dispersion can be calculated. The model is developed using Fresnel diffraction theory. Here we calculate the temperature co-efficient of refractive index (dn/dT) for the MoS_2 dispersion samples which are diluted by series two-fold dilution three times. According to the model, the temporal change in the TL signal is given by

$$I(t) = I(0)\left\{1 - \frac{\theta}{2}\arctan\left[\frac{2mV}{\left[(1+2m)^2 + V^2\right]\left(\frac{t_c}{2t}\right) + 1 + 2m + V^2}\right]\right\}^2 \quad (1)$$

Here.

$I(0)$- intensity of the TL signal when either t or θ is zero

ω_{0p} – probe beam waist radius = 6.31 μm

ω_{1p} – probe beam radius at the sample = 5.75 mm. ω_e – pump beam waist radius = 18.93 μm

$$V = \frac{Z_1}{Z_c} = \frac{\textit{Probe beam waist to sample distance}}{\frac{\pi\omega_{0p}{}^2}{\lambda_p}} = \frac{21.5*10^{-2}}{1.9244*10^{-4}} = 1117.23$$

$$m = \left(\frac{\omega_{1p}}{\omega_e}\right)^2 = 92264.46$$

After fitting equation (1) to experimental TL signal data, we can get values of constants t_c and θ. Parameter t_c is a characteristic time constant which depends on properties of dispersion like specific heat and density. Parameter θ is a dimensionless variable which depends on strength of thermal lens. It is approximately equal to thermally induced phase shift of probe beam between center and edge of dark spot at steady state of thermal lens. Further, we can calculate the temperature coefficient of the refractive index, $\frac{dn}{dT} = \frac{-\theta K \lambda_p}{PAL\phi}$.

Here.

K - thermal conductivity of the dispersion = ~0.1769W/mK [22].

P - pump beam (excitation) power = 30 mW.

A - absorption co-efficient of the dispersions = 68.097 m^{-1}

L-sample thickness = 1.5 mm

ϕ-fraction of excitation energy converted into heat = 1.

Negative sign of dn/dT is due to negative photothermal lens generated by the pump beam within the sample. Assuming that the thermal conductivity (K) and absorption co-efficient (A) are not changing significantly with concentration of MoS_2 nanoflakes, dn/dT is calculated. The trend of dn/dT is shown in Fig. 8.

With dilution higher than 1/2, small peaks are observed in the TL signal just after formation of the thermal lens. These peaks are due to perturbation in dispersions. A possible explanation for this is that with higher dilution, the concentration of the MoS_2 nanoflakes is lower and there is a weak thermal lens formation. Hence the photothermal lens formed gets easily distorted by weak convective flows. Since the TL signal has already reached lowest point, datapoints in these peaks (greyed out data points in Fig. 7) are masked and not considered for the

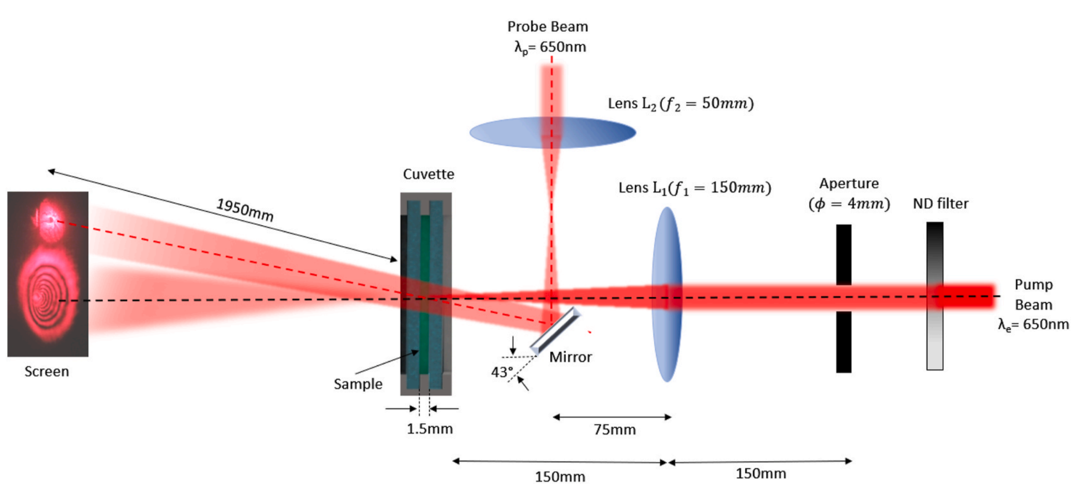

Fig. 3. Experimental setup to study time evolution and quantification of thermal lens region. (distance between L_2 to Beam splitter = 18 cm).

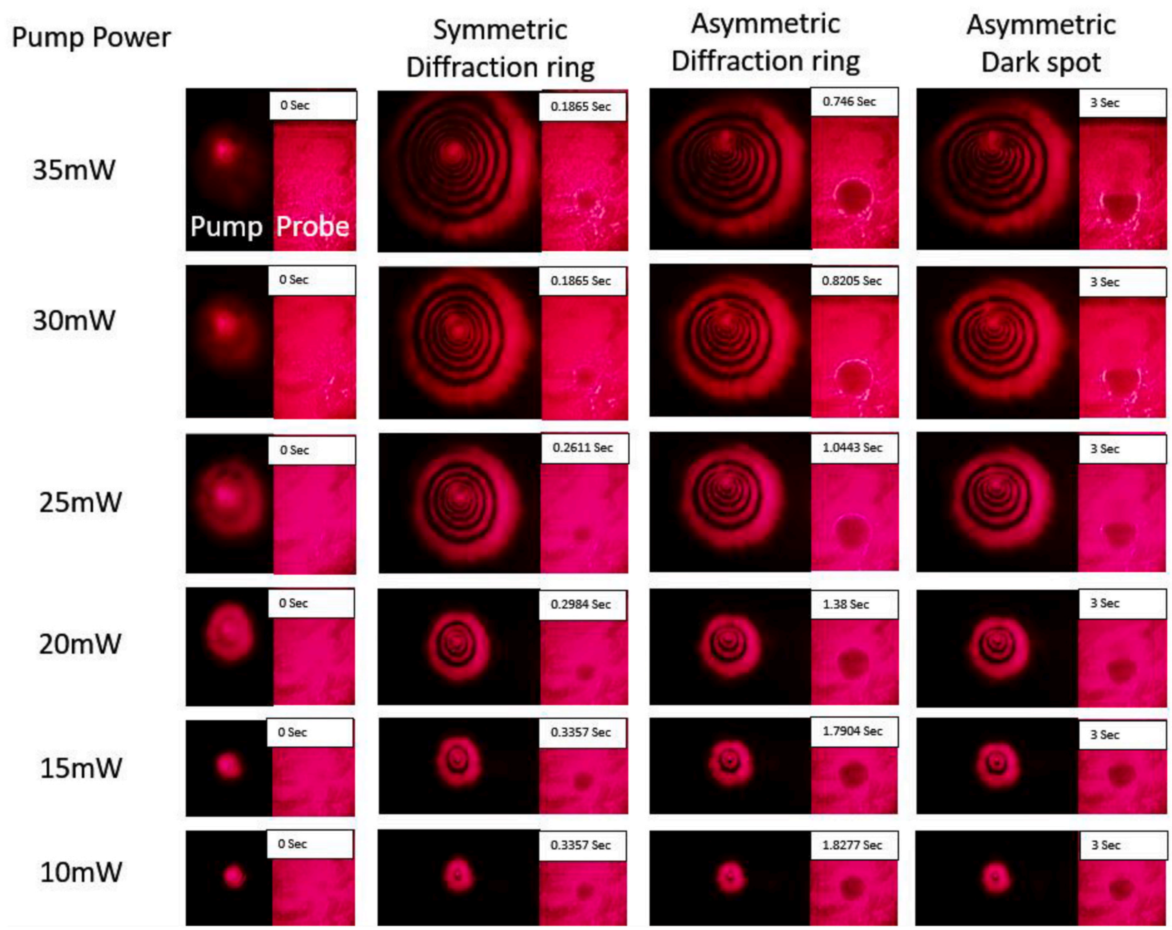

Fig. 4. Time evolution of diffraction rings and thermal lens dark spot for different pump power (inset: Elapsed time). See supplementary material for video.

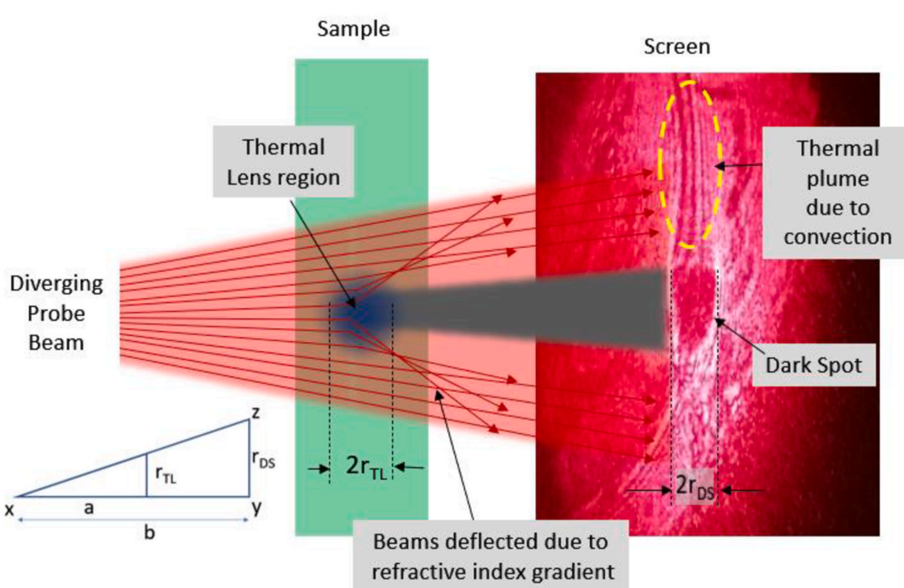

Fig. 5. Light rays from the probe beam which encounter thermal lens region get deflected due to refractive index gradient.

model fit. Table 2 shows the values of constants t_c and θ extracted from the experimental data by fitting to the model as shown in Fig. 7.

Temperature dependent change in the refractive index (dn/dT) is found to decrease with increase in dilution of the MoS_2 dispersion (Fig. 8). This dependency can be explained as follows: large surface area of MoS_2 nanoflakes allows higher absorption of light as well as efficient transfer of heat to other molecules. At higher concentration of MoS_2 nanoflakes (i.e. at lower dilution of dispersion), there is greater absorption of the pump beam and more nanoflakes act as a heat source. Further, this heat gets absorbed by the neighboring solvent molecules

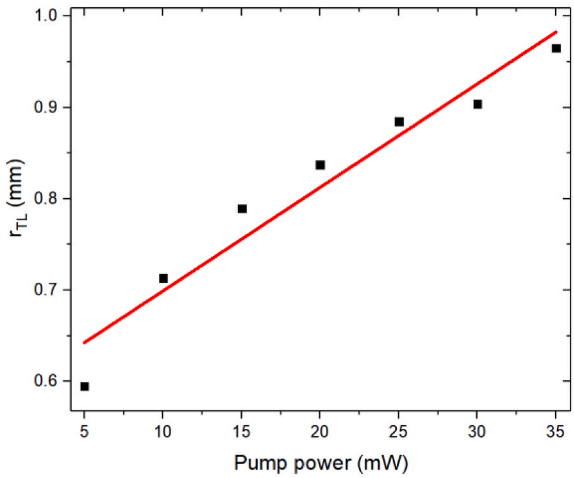

Fig. 6. Dependence of the thermal lens size on the pump power.

causing large refractive index gradient. Thermo-optic coefficient (dn/dT) of nano layer MoS_2 is reported as $\sim 10^{-5} K^{-1}$ [23,24] · Whereas of common solvent (ethanol) is ~ $-10^{-4} K^{-1}$ [25]. In this research thermo-optic coefficient of MoS_2 nanoflakes dispersion is measured to be ~ $-3.66 \times 10^{-5} K^{-1}$ and decreases up to ~ $-1.03 \times 10^{-5} K^{-1}$ after dilution to 1/8th of initial concentration. This indicates the effective thermo-optic co-efficient of MoS_2 nanoflakes dispersion depends primarily on dn/dT of solvent and proportional to MoS_2 nanoflakes concentration. Hence thermo-optic properties of the MoS_2 dispersions can be optimized by changing the concentration of MoS_2 nanoflakes and the solvent.

Fig. 9 shows the experimental setup to demonstrate MoS_2 dispersions as prospective material for the "normally on" all optical switch. The three terminals of the optical switch comprise of two input beams i.e. the pump and probe beams, and the part of the diverging probe beam transmitted through the thermal lens region in dispersion. The latter is considered as the output. To avoid heating of the proposed device, the wavelength of probe beam should be chosen to have least absorbance by the dispersion. The thermal lens is created by focusing the pump beam using lens L_1. Beam powers are controlled by using a variable Neutral Density (ND) filter and measured using PM320E Thorlabs optical power meter with a Si photodiode as a sensor. By keeping the probe power constant, the output power is measured by the varying pump power from 0 to 70 mW in step of 5 mW increment. Measurements are repeated for four different probe powers from 5 to 25mw.

Fig. 10 shows output characteristics of the thermo-optic refraction based all optical switch. This graph looks very similar to the output characteristics of the conventional electronic transistor. The output switch-off time for the probe power of 25 mW and pump power of 30 mW is found to be ~0.16 s. We deduce following conclusions from Fig. 10(inset): the amplitude of the output power when the pump power is zero can be controlled by the probe beam power. The slope of the linear response in the output power below 15mw of the pump power can be increased by increasing the probe power. Therefore, there is good control over modulation of output signal in thermo-optic refraction based approach for optical switching.

The present configuration contains MoS_2 in colloidal form where there is a limitation in response time due to solvent. In real life application the demonstrated concept (thermo-optic refraction in MoS_2) in this research should be applied as a single/few layer MoS_2 (solid state) sandwiched between micro laser (pump) and substrate. A second micro laser orthogonal to this arrangement can act as probe. In this micro

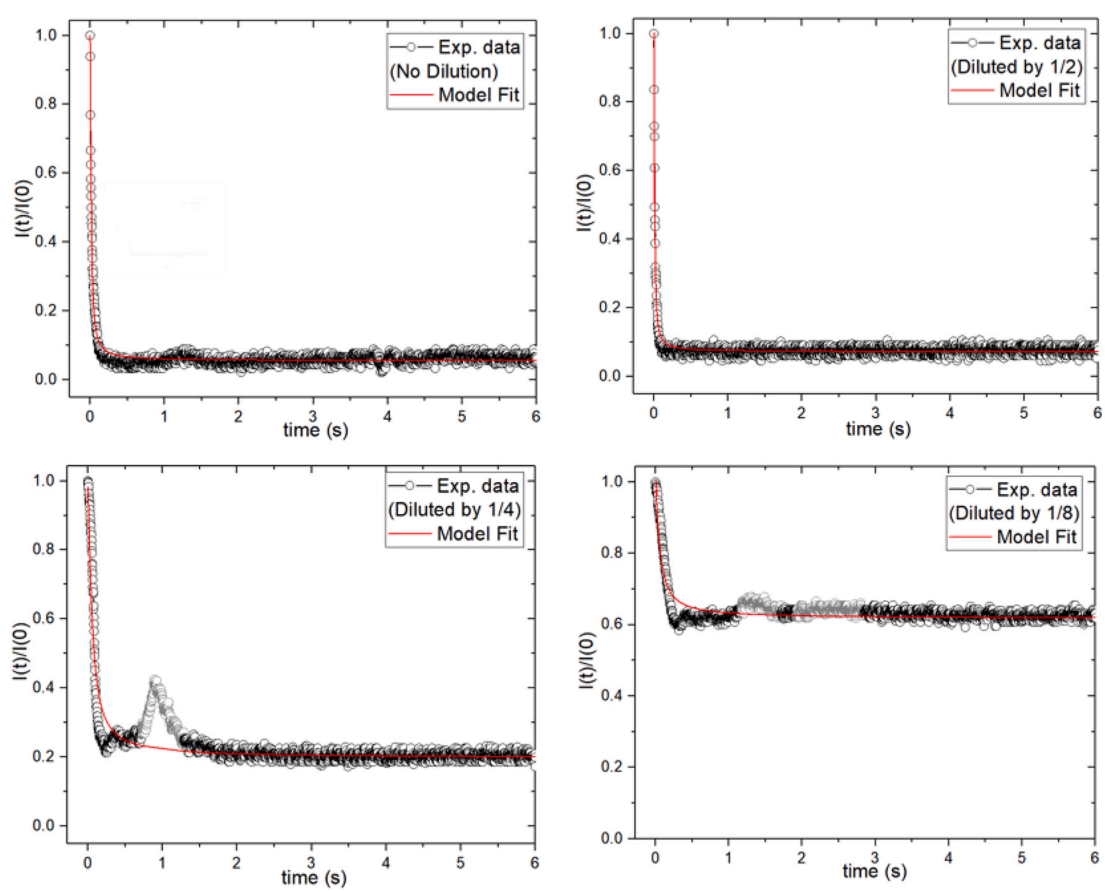

Fig. 7. Thermal lens signal variation with time for different dilution of the sample (greyed out sample points are not considered for model fit).

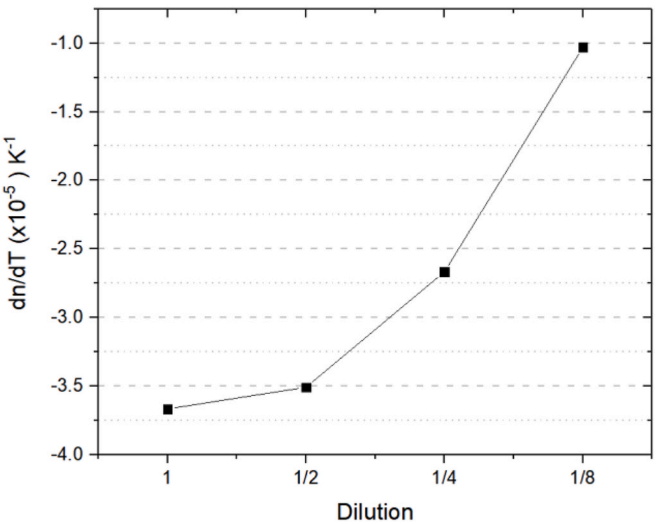

Fig. 8. Change in thermal co-efficient of refractive index (dn/dT) for two-fold series dilution of MoS_2 dispersions.

Table 2
Constants t_c and θ extracted by fitting the model to thermal lens experimental data as shown in Fig. 7 for different dilution of MoS_2 dispersions.

Dilution	t_c (msec)	θ
0	0.29	0.9774
1/2	0.1767	0.9348
1/4	0.9494	0.7109
1/8	0.8568	0.27393

device one can expect better parameters liker higher switching speed and low power.

3. Conclusion

In this work we visually studied the time evolution of the thermal lens (TL) region in MoS_2 dispersions by pump-probe configuration. It is visually confirmed that there is a collapse of diffraction rings of the transmitted pump beam due to a vertical convective heat flow. Size of the TL region is reduced by 38.4% when the pump power is varied from 35 to 5 mW. The thermo-optic properties of MoS_2 dispersions were studied using TLS technique. It is found that the temperature coefficient of the refractive index increases with increase in concentration of MoS_2 nanoflakes in the dispersion. By considering thermo-optic refraction as a tool for optical modulation, a 'normally on' all optical switch is demonstrated using MoS_2 dispersions. There is an excellent modulation of output beam using the pump beam. Low power micro-optical devices based on single monolayer MoS_2 can be explored in future work.

CRediT authorship contribution statement

Pritam P. Shetty: Conceptualization, Investigation, Methodology, Validation, Visualization, Writing - original draft. **Mahalingam Babu:** Investigation. **Dmitrii N. Maksimov:** Writing - review & editing. **Jayachandra Bingi:** Conceptualization, Methodology, Writing - review & editing, Supervision.

Declaration of competing interest

The authors declare that they have no known competing financial interests or personal relationships that could have appeared to influence

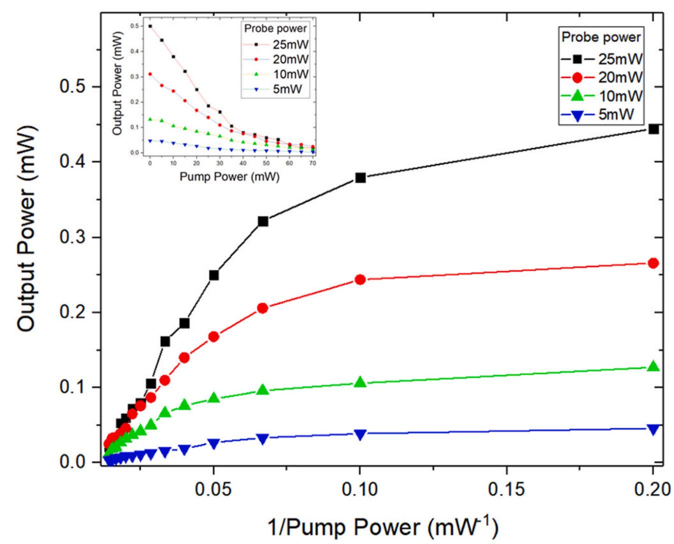

Fig. 10. Output characteristics of the "normally on" all optical switch shows output power variation vs 1/(input pump power), inset-output power vs input pump power.

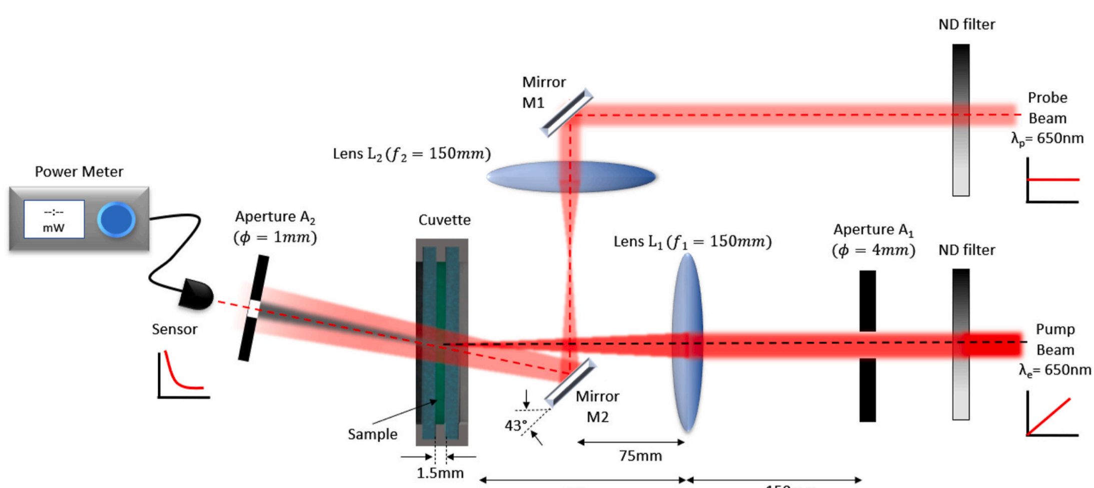

Fig. 9. Experimental setup for "normally on" all optical switch (distance between L_2 and M_2 = 18 cm, A_2 and sample = 5 cm). Pump beam emerging out of the sample inthe cuvette is not shown.

the work reported in this paper.

Acknowledgements

Authors acknowledge the funding support from DST India under INT/RUS/RFBR/P-262.

Appendix A. Supplementary data

Supplementary data to this article can be found online at https://doi.org/10.1016/j.optmat.2020.110777.

References

[1] X. Li, H. Zhu, Two-dimensional MoS2: properties, preparation, and applications, J. Mater. 1 (1) (2015) 33–44, https://doi.org/10.1016/j.jmat.2015.03.003.
[2] A. Abareshi, M. Arshadi Pirlar, M. Houshiar, Photothermal property in MoS2 nanoflakes: theoretical and experimental comparison, Mater. Res. Express 6 (2019) 10, https://doi.org/10.1088/2053-1591/ab3810.
[3] A.A. Tedstone, et al., Mechanical properties of molybdenum disulfide and the effect of doping: an in situ TEM study, ACS Appl. Mater. Interfaces 7 (37) (2015) 20829–20834, https://doi.org/10.1021/acsami.5b06055.
[4] T. Han, et al., Probing the optical properties of MoS2 on SiO2/Si and sapphire substrates, Nanomaterials 9 (5) (2019), https://doi.org/10.3390/nano9050740.
[5] J.Y. Wu, M.N. Lin, L. De Wang, T. Zhang, Photoluminescence of MoS2 prepared by effective grinding-assisted sonication exfoliation, J. Nanomater. 2014 (2014), https://doi.org/10.1155/2014/852735.
[6] K.F. Mak, C. Lee, J. Hone, J. Shan, T.F. Heinz, Atomically thin MoS2: a new direct-gap semiconductor, Phys. Rev. Lett. 105 (13) (2010) 2–5, https://doi.org/10.1103/PhysRevLett.105.136805.
[7] G.L. Biosensors, et al., MoS 2 field-E ff ect transistor for next-, ACS Nano Xx (2014) 3992–4003, https://doi.org/10.1021/nn5009148.
[8] S. Wachter, D.K. Polyushkin, O. Bethge, T. Mueller, A microprocessor based on a two-dimensional semiconductor, Nat. Commun. 8 (2017) 1–6, https://doi.org/10.1038/ncomms14948.
[9] B.P. Majee, S. Mishra, R.K. Pandey, R. Prakash, A.K. Mishra, Multifunctional few-layer MoS2 for photodetection and surface-enhanced Raman spectroscopy application with ultrasensitive and repeatable detectability, J. Phys. Chem. C 123 (29) (2019) 18071–18078, https://doi.org/10.1021/acs.jpcc.9b04279.
[10] B. Han, Y.H. Hu, MoS2 as a co-catalyst for photocatalytic hydrogen production from water, Energy Sci. Eng. 4 (5) (2016) 285–304, https://doi.org/10.1002/ese3.128.
[11] S. Karmakar, S. Biswas, P. Kumbhakar, Low power continuous-wave nonlinear optical effects in MoS2 nanosheets synthesized by simple bath ultrasonication, Opt. Mater. (Amst). 73 (2017) 585–594, https://doi.org/10.1016/j.optmat.2017.09.020.
[12] J.W. You, S.R. Bongu, Q. Bao, N.C. Panoiu, Nonlinear optical properties and applications of 2D materials: theoretical and experimental aspects, Nanophotonics 8 (1) (2018) 63–97, https://doi.org/10.1515/nanoph-2018-0106.
[13] J. Sun, et al., Synthesis methods of two-dimensional MoS2: a brief review, Crystals 7 (7) (2017) 1–11, https://doi.org/10.3390/cryst7070198.
[14] T. Neupane, B. Tabibi, F.J. Seo, Spatial self-phase modulation in WS 2 and MoS 2 atomic layers, Opt. Mater. Express 10 (4) (2020) 831, https://doi.org/10.1364/ome.380103.
[15] S. Xiao, B. Lv, L. Wu, M. Zhu, J. He, S. Tao, Dynamic self-diffraction in MoS_2 nanoflake solutions, Optic Express 23 (5) (2015) 5875, https://doi.org/10.1364/oe.23.005875.
[16] L. Wu, et al., Recent Advances of Spatial Self-phase Modulation in 2D Materials and Passive Photonic Device Applications, 2020, pp. 1–22, https://doi.org/10.1002/smll.202002252, 2002252.
[17] X. jun Zhang, et al., A review on spatial self-phase modulation of two-dimensional materials, J. Cent. South Univ. 26 (9) (2019) 2295–2306, https://doi.org/10.1007/s11771-019-4174-8.
[18] Y. Wu, et al., Emergence of electron coherence and two-color all-optical switching in MoS2 based on spatial self-phase modulation, Proc. Natl. Acad. Sci. U. S. A 112 (38) (2015) 11800–11805, https://doi.org/10.1073/pnas.1504920112.
[19] Y. Jia, et al., Nonlinear optical response, all optical switching, and all optical information conversion in NbSe 2 nanosheets based on spatial self-phase modulation, Nanoscale 11 (10) (2019) 4515–4522, https://doi.org/10.1039/c8nr08966c.
[20] Y.K. Srivastava, et al., MoS2 for ultrafast all-optical switching and modulation of THz fano metaphotonic devices, Adv. Opt. Mater. 5 (2017) 23, https://doi.org/10.1002/adom.201700762.
[21] J. Shen, R.D. Lowe, R.D. Snook, A model for cw laser induced mode-mismatched dual-beam thermal lens spectrometry, Chem. Phys. 165 (2–3) (1992) 385–396, https://doi.org/10.1016/0301-0104(92)87053-C.
[22] G. Cai, H. Zong, Q. Yu, R. Lin, Thermal conductivity of alcohols with acetonitrile and N,N-dimethylformamide, J. Chem. Eng. Data 38 (2) (1993) 332–335, https://doi.org/10.1021/je00010a038.
[23] H.L. Liu, et al., "Temperature-dependent optical constants of monolayer MoS 2 , MoSe 2 , WS 2 , and WSe 2 : spectroscopic ellipsometry and first-principles calculations, Sci. Rep. 10 (1) (2020), https://doi.org/10.1038/s41598-020-71808-y.
[24] Y. Zhang, L. Tao, D. Yi, J. Bin Xu, H.K. Tsang, Enhanced thermo-optic nonlinearities in a MoS2-on-silicon microring resonator, Appl. Phys. Express 13 (2) (2020) 2–6, https://doi.org/10.7567/1882-0786/ab626c.
[25] R.C. Kamikawachi, et al., Determination of thermo-optic coefficient in liquids with fiber Bragg grating refractometer, Optic Commun. 281 (4) (2008) 621–625, https://doi.org/10.1016/j.optcom.2007.10.023.